Viscoelastic Properties of Entangled Polymers. I. The Elastically Coupled Entanglement Model

David R. Hansen, Michael C. Williams, and Mitchel Shen*

Department of Chemical Engineering, University of California, Berkeley, California 94720. *Received September 22, 1975*

ABSTRACT: The bead and spring model of Rouse, Bueche, and Zimm is extended to describe the viscoelastic behavior of polymers with chain entanglements. Motion of the macromolecules is retarded by the presence of entanglements with neighboring chains. This effect is in part represented by selected beads along the chain having enhanced friction coefficients. These selected beads may have values of friction coefficients that are uniformly higher than the unentangled beads, or are progressively higher as a function of the position along the chain. Major improvements in the model result when these entangle points are also assumed to be elastically coupled to the surrounding medium. This coupling is modeled by interconnecting the entangled beads with springs having low spring constants. The resulting equations of motion of the model contain a modified Zimm matrix that is nonsymmetrical. The eigenvalues were obtained numerically on the computer to yield the relaxation spectra, permitting calculation of dynamic moduli, relaxation moduli, steady-state shear compliance, and zero-shear viscosity for a series of molecular weights. Agreement with experimental data on monodisperse polystyrene was found to be excellent for all these properties. Of particular interest is the ability of the model to predict the equilibrium shear compliance as a function of molecular weight, which was not achievable by earlier theories. The sensitivity of J_{eR} to the fitting parameters renders it a useful discriminator in selecting the best model for describing chain entanglement effects in polymer viscoelasticity.

It has long been recognized that rheological properties of polymers, in bulk or concentrated solution, manifest a rather abrupt qualitative transition in form when molecular weight M exceeds a critical value M_c. This transition is customarily explained in terms of the entanglement concept, which postulates that a transient polymer network can be formed when each molecule experiences at least two loop-like entanglements with nearby molecules which impede its response to deformation. A number of reviews have been published on this subject.[1-3]

The molecular theory of viscoelasticity expounded by Rouse,[4] Bueche,[5] and Zimm[6] has been eminently successful in applications to polymers with $M < M_c$. Above M_c, however, the theory is unable to predict many of the viscoelastic functions, as shown in Table I. Numerous authors have proposed modifications to the basic RBZ model in order to remove the observed discrepancies. In this work, we shall present a relatively simple method for modeling and interpreting entanglement phenomena which provides the capability of fitting all the data in Table I, i.e., the molecular weight and frequency dependence of the dynamic moduli, $G'(\omega)$ and $G''(\omega)$, the molecular weight and time dependence of relaxation modulus, $E_r(t)$, as well as the molecular weight dependence of steady-state shear compliance, J_e, and zero-shear viscosity, η_0.

Theory

1. The Enhanced Friction Model. The Rouse–Bueche–Zimm (RBZ) theory represents the polymer molecule by $N + 1$ beads (frictional centers) held together with N entropy springs. The equation of motion for such a system is, for x components:[4-6]

$$\dot{\mathbf{x}} = \mathbf{v}_x{}^s - \mathcal{D}\frac{\partial \ln \psi}{\partial \mathbf{x}} - \sigma \mathbf{Z}\cdot\mathbf{x} \qquad (1)$$

In eq 1, $\mathbf{x}$ and $\dot{\mathbf{x}}$ are column vectors of bead positions and bead velocities respectively, $\mathbf{v}_x{}^s$ is the solvent velocity, $\mathcal{D} = kT/f$ is the diffusion coefficient, $\partial \ln \psi/\partial \mathbf{x}$ is the gradient of the configurational potential, $\mathbf{Z}$ is the nearest neighbor Zimm matrix, and $\sigma = 3kT/b^2f$ where b^2 is the average end-to-end distance of the submolecule and f is the frictional coefficient. Equation 1 poses an eigenvalue problem whose solution yields the distribution of relaxation (or retardation) times for the system, from which the rheological properties of the polymer can be readily obtained for homopolymers without entanglement.

When $M > M_c$, both the magnitude and the distribution of relaxation times are substantially affected by the presence of entanglements. Bueche[7] first suggested that the effect of entanglements can be explained in terms of the enhanced friction coefficients. More refined molecular theories were subsequently published by Ferry,[8] Chömpff,[9,10] DeGennes,[11] Vinogradov,[12] and their coworkers. In addition, a phenomenological treatment has been given by Marvin and Oser.[13]

In previous publications we have modified the RBZ theory for the computation of relaxation spectra of block copolymers.[14-16] The block copolymers were modeled by strings of beads of different friction coefficients. This model can be readily adapted for entangled polymers, which can be represented by a string of low-friction (unentangled, or fast) beads among which are dispersed high-friction (entangled, or slow) beads. If we designate the high-friction beads as "A beads", and low-friction beads as "B beads", then the equation of motion can be written as

$$\dot{\mathbf{x}} = \mathbf{v}_x{}^s - \mathcal{D}_B\mathbf{D}^{-1}\cdot\frac{\partial \ln \psi}{\partial \mathbf{x}} - \sigma_B\mathbf{D}^{-1}\cdot\mathbf{Z}\cdot\mathbf{x} \qquad (2)$$

where $\sigma_B = 3kT/b_B{}^2f_B$, $\mathcal{D}_B = kT/f_B$, and $\mathbf{D}^{-1}$ is the inverse matrix of

$$\mathbf{D} = \begin{bmatrix} 1 & & & & & & \\ & 1 & & & & & \\ & & \ddots & 1_{\delta_A} & & & \\ & & & 1 & \ddots & 1_{\delta_A} & \\ & & & & & 1 & \ddots \\ & & & & & & 1 \end{bmatrix} \qquad (3)$$

with $\delta_A = f_A/f_B$. The distribution of δ_A's along the diagonal of $\mathbf{D}$ identifies the positions of entangled points in the polymer molecule. Although Z is a tridiagonal symmetrical matrix, the product $\mathbf{D}^{-1}\cdot\mathbf{Z}$ is not. The eigenvalue spectrum of the latter can nevertheless be readily obtained numerically on the computer by the use of a subroutine for nonsymmetrical matrices available at the University of California Computer Center.

The entanglement positions will here be taken to be located at regular intervals along the chain, an assumption which is computationally convenient and facilitates com-

Table I
Linear Properties of Bulk Polymers

Property	Definition	Reduced form	Obsd when $M \geq M_c$	Rouse prediction[a]
Low-shear viscosity $\eta_0(M)$	$\frac{\rho RT}{M}\sum_p \tau_p$	$\frac{1}{N_e}\sum_p \tau_p'$	$\sim M^{3.3}$ to $M^{4.0}$	$\sim M$
Steady-state compliance; reduced $J_{eR}(M)$	$\frac{\sum_p \tau_p^2}{(\sum_p \tau_p)^2}$	$\frac{\sum_p \tau_p'^2}{(\sum_p \tau_p')}$	$0.4 < J_{eR} < 0.8$ when $M \leq M_c$ $1/M$ when $M > M_c$	0.4
Max relaxation time $\tau_m(M)$	$\frac{\eta_0 M}{\rho RT}\frac{1}{\lambda_1 \sum_p \lambda_p^{-1}}$	ϕ_A^2/λ_1	$\sim M^{3.3}$ to $M^{4.0}$ $\sim \eta_0$	$\sim M^2$ $\sim \eta_0 M$
Storage modulus $G'(\omega)$	$\frac{\rho RT}{M}\sum_p \frac{\omega^2\tau_p^2}{1+\omega^2\tau_p^2}$	$\frac{1}{N_e}\sum_p \frac{\omega^2\tau_p'^2}{1+\omega^2\tau_p'^2}$	Rubbery plateau of width $\sim M^{2.3}$ to $M^{3.0}$, with abrupt drop in terminal zone	No plateau, $G' \sim \omega^{1/2}$
Loss modulus $G''(\omega)$	$\frac{\rho RT}{M}\sum_p \frac{\omega\tau_p}{1+\omega^2\tau_p^2}$	$\frac{1}{N_e}\sum_p \frac{\omega\tau_p'}{1+\omega^2\tau_p'^2}$	Plateau with a *minimum* at higher ω	No plateau, $G'' \sim \omega^{1/2}$
Relaxation[b] modulus $G_r(t)$	$\frac{\rho RT}{M}\sum_p e^{-t/\tau_p}$	$\frac{1}{N_e}\sum_p e^{-t/\tau_p'}$	Rubbery plateau of width $\sim M^{2.3}$ to $M^{3.0}$, with abrupt drop in terminal zone	No plateau, $G \sim t^{-1/2}$

[a] Useful for bulk polymers ($\eta_S \ll \eta_0$) in the absence of entanglements [b] For rubbery polymers $E_r = 3G_r$, which is used for computing the curves in Figures 13 and 14.

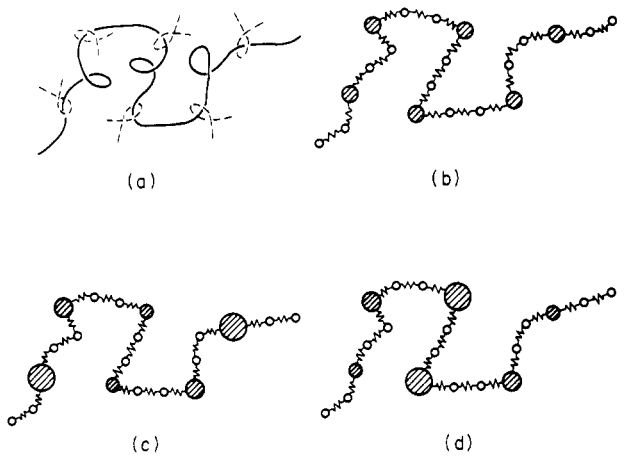

Figure 1. Schematic representations of entangled polymer chains. (a) Parent chain (solid line) entangled with passing chains (broken lines); (b) entangled points are represented by slow (shaded) beads with *uniformly enhanced* friction coefficients (indicated by sizes of the shaded beads in comparison with the unshaded or unentangled beads); (c) entangled points are represented by slow beads with *decreasing* friction coefficients toward the interior of the chain; (d) entangled points are represented by slow beads with *increasing* friction coefficients toward the interior of the chain.

parison among the different cases. Realistically, of course, the entangled points are probably randomly distributed along the macromolecule, but the need to introduce such subtleties is dubious. As partial justification of constant spacing, we might consider these slow beads as time or position averaged "effective" entanglement points.

Figure 1 shows the entanglement points as large shaded beads along the chain. Sizes of the beads refer only to the magnitudes of the friction coefficients, and not to the masses of the beads which are all equivalent. The simplest case here is the chain containing slow beads with uniformly enhanced friction coefficients (Figure 1b). However, the values of δ_A can vary as a function of molecular weight, or as a function of the number of entangled beads (N_e):

$$\delta_A = \alpha N_e^{\beta} \tag{4}$$

where α and β are constants. Chömpff and Prins[10] as well as Vinogradov and coworkers[12] used a model with the values of the friction coefficients of the slow beads varying as a function of position along the chain (Figure 1c). The entanglements situated near the ends of the chain were given the highest friction coefficient with values of δ_A varying according to the following relation:

$$\delta_A(I) = aI^b$$
$$I = 1, 2, 3, \ldots, N_e/2 \quad (N_e \text{ even}) \tag{5}$$
$$I = 1, 2, 3, \ldots, (N_e + 1)/2 \quad (N_e \text{ odd})$$

where I refers to the number of the slow beads. Counting is initiated from the center bead(s) and progresses toward the two chain ends. In eq 5, a and b are constants. An alternate model is shown in Figure 1d, where the slowest beads are situated in the chain middle. Equation 5 still applies, but now the counting begins from the chain ends toward the chain middle. This latter distribution appears to be more reasonable in that entanglements near the ends may be more easily disentangled than those in the middle, and that the chain ends usually are more mobile. In this work, all three models will be examined and the results compared with each other.

Although this model is conceptually similar to those proposed previously, it is much simpler to use. For example, the rather complex procedure of "decoupling" in the Chömpff theory is circumvented. In addition, we have indicated in our previous paper[16] that small (~20 × 20) matrices may be used for these computations with the same result as larger matrices. The resulting economy and efficiency permit us to examine a large number of cases for comparison.

2. The Elastic Coupling Model. The enhanced friction model described above only accounts for the retardation of the molecular motion of the macromolecule due to drag force imposed by the entanglements. However, as shown in Figure 2a, as the slow bead moves through the medium it must also pull along the neighboring molecule that is entangled with the central molecule. As a consequence, an elastic force must be developed at the point of entanglement. It is well known in the theory of rubber elasticity that such entanglements may be considered to be temporary physical crosslinks.[17] When there are sufficient such

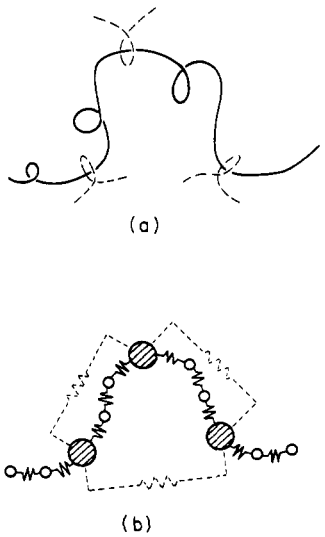

Figure 2. Schematic representations of elastically coupled entangled chains. The parent chain (solid line) entangled with three passing chains (broken lines) in (a) is modeled by (b) where the springs drawn by broken lines interconnect all the entangled points.

crosslinks in the system, a rubbery plateau region will appear in the viscoelastic master curve due to the formation of an infinite network structure. Thus at a given entanglement point, that slow bead is elastically coupled not only to the neighboring bead, on the parent chain, but also to the medium through this network structure. The medium transmits this elastic force weakly to other beads on the parent molecule. We here model this coupling effect by interconnecting each slow bead in the macromolecule to every other slow bead on the same chain through weak entropy springs (Figure 2b). Crudely, this intramolecular elastic coupling can be viewed as analogous to the intramolecular viscous coupling ("hydrodynamic interaction") introduced by Zimm[6] for dilute solutions.

The force balance equation for the unentangled B beads can be written as follows:

$$\dot{x}_k{}^{\mathrm{B}} = v_{x_k}{}^{\mathrm{s}} - \left(\frac{kT}{f_{\mathrm{B}}}\right)\left(\frac{\partial \ln \psi}{\partial x_k}\right) + \left(\frac{3kT}{f_{\mathrm{B}} b_{\mathrm{B}}{}^2}\right)(x_{k-1} - 2x_k + x_{k+1}) \quad (6)$$

where $k \neq 0, N$. Because of the additional elastic coupling with the medium, the equation for entangled A beads must be of the following form (with $b_{\mathrm{A}}{}^2 = b_{\mathrm{B}}{}^2$):

$$\dot{x}_j{}^{\mathrm{A}} = v_{x_j}{}^{\mathrm{s}} - \left(\frac{kT}{f_{\mathrm{A}}}\right)\left(\frac{\partial \ln \psi}{\partial x_j}\right) + \left(\frac{3kT}{f_{\mathrm{A}} b_{\mathrm{B}}{}^2}\right)(x_{j-1} - 2x_j + x_{j+1}) - \left(\frac{3kT}{f_{\mathrm{A}} b_{\mathrm{B}}{}^2}\right)\left[\epsilon \sum_{i=1}^{N_e}(x_j - x_{\nu i})\right] \quad (7)$$

where $j \neq k \neq 0$ or N. In eq 7, subscript j is the usual position index ($j = 3, 6, \ldots$ for A beads in Figure 1) while i is the index for slow beads alone, ν defines the spacing frequency of the entangle points (e.g., $\nu = 3$ in Figure 1) such that $N + 1 = \nu(N_e + 1) - 1$. Equation 7 also introduces ϵ as a measure of the strength of the spring constant coupled to the medium:

$$\epsilon = \left(\frac{3kT}{f_{\mathrm{A}} b_e{}^2}\right) \Big/ \left(\frac{3kT}{f_{\mathrm{A}} b_{\mathrm{A}}{}^2}\right) = \frac{b_{\mathrm{A}}{}^2}{b_e{}^2} \quad (8)$$

where $b_e{}^2$ may be considered the average end-to-end distance of the "effective" submolecule connecting two slow beads through the infinite network structure formed through entanglement coupling. Since the coupling must be effected through a rather circuitous route in the network, $b_e{}^2$ can be expected to be much longer than $b_{\mathrm{A}}{}^2$. The entropy spring for this type of coupling is therefore much weaker than the "normal" entropy springs, and ϵ is a small number.

Expressed in matrix notation, the equation of motion for the elastically coupled model can be written as

$$\dot{\mathbf{x}} = \mathbf{v}_x{}^{\mathrm{s}} - \mathcal{D}_{\mathrm{B}}\mathbf{D}^{-1} \cdot \frac{\partial \ln \psi}{\partial \mathbf{x}} - \sigma_{\mathrm{B}}\mathbf{D}^{-1} \cdot \mathbf{Z}_c \cdot \mathbf{x} \quad (9)$$

where $\mathbf{Z}_c$ is the "coupled" Zimm matrix. As an example, for a chain in which every other bead is a slow bead ($\nu = 2$) the form of $\mathbf{Z}_c$ can be given by eq 10:

$$\mathbf{Z}_c = \begin{bmatrix} 1 & -1 & 0 & 0 & 0 & 0 & \cdots \\ -1 & 2+\gamma & -1 & -\epsilon & 0 & -\epsilon & \cdots \\ 0 & -1 & 2 & -1 & 0 & 0 & \cdots \\ 0 & -\epsilon & -1 & 2+\gamma & -1 & -\epsilon & \cdots \\ 0 & 0 & 0 & -1 & 2 & -1 & \cdots \\ 0 & -\epsilon & 0 & -\epsilon & -1 & 2+\gamma & \cdots \\ \vdots & \vdots & \vdots & \vdots & \vdots & \vdots & \vdots \end{bmatrix} \quad (10)$$

where $\gamma = (N_e - 1)\epsilon$.

Conceptually the elastic coupling model is similar to those previously proposed by Graessley[18] and by Forsman and Grand.[19] Graessley assumed the coupling of the slow beads to take place through connection to the center of gravity of a chain passing by the parent chain. The coupling coefficient used by Forsman and Grand, although physically not explicitly defined, is mathematically analogous to our strength ratio of entropy springs (ϵ) given in eq 8. These latter authors solved their force balance equations by imposing symmetry constraints on the entanglements, and found that the principal effect of entanglements is to increase some of the longest odd-order relaxation times.

Computational Details

In order to remove the arbitrariness in the specific choices of the number of beads in our computation, we shall use several reduced quantities in presenting the results of our computations. We have found that the results of the computed relaxation spectra are insensitive to the actual sizes of the matrices when the total number of beads is approximately 20 or greater. Thus it is not necessary to simulate the actual molecular weights of the polymers by using very large matrices, such as the 500 × 500 matrices employed by Chömpff and Prins.[10] The polymer molecule can be simulated by much smaller matrices if δ_{A} and ϵ are adjusted to compensate for the different submolecule sizes. The submolecule size, of course, is a function of the number of beads. In other words, it fixes the size of the matrix for a given molecular weight. The frictional coefficient ratio, $\delta_{\mathrm{A}} = f_{\mathrm{A}}/f_{\mathrm{B}}$, will be a function of f_{B} which is equal to $m\zeta \propto M/(N+1) \propto N_e/(N+1)$ where m is the number of monomer units in the bead and ζ is the monomeric friction coefficient.[2] If one assumes that the physical point of entanglement is always within the designated submolecule, independent of the submolecule size, then f_{A} is constant. Therefore, δ_{A} is proportional to $(N+1)/N_e$. The validity of this relationship is shown in Figure 3 in the plot of log $(\tau_m/\tau_m{}^0)$ vs. log $\delta_{\mathrm{A}}\phi_{\mathrm{A}}$ where the fraction of entanglement beads is $\phi_{\mathrm{A}} = N_e/(N+1)$, $\tau_m{}^0$ is the maximum relaxation time with no high-frictional beads in the molecule, and τ_m is that for a chain in which every other bead is a slow bead.

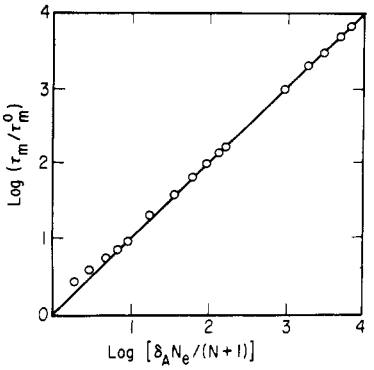

Figure 3. Double logarithmic plot of the ratio of maximum relaxation times of a chain with alternating fast and slow beads ($\nu = 2$) to that with fast beads only (unentangled polymer) vs. $\delta_A N_e/(N+1)$ or $\delta_A\phi_A$.

The slope of unity indicates that τ_m is proportional to $\delta_A\phi_A$ for a wide range of $\delta_A\phi_A$. There is some deviation, however, at small values of $\delta_A\phi_A$. The other relaxation times are generally affected in a similar manner, so that calculated viscoelastic functions for different size matrices are indistinguishable.

Because δ_A must vary with ϕ_A, for convenience we shall define the reduced frictional coefficient enhancement ratio as:

$$\delta_A' = \delta_A N_e/(N+1) \tag{11}$$

which is independent of the size of the matrix. The δ_A used and the actual calculations in the **D** matrix can be easily obtained from eq 11 for any size matrix.

In the same spirit, we shall define a reduced spring constant strength ratio, ϵ'. The length of the submolecule in the chain is

$$b_A^2 = b_B^2 = \langle r^2\rangle/N \propto M/N \tilde{\propto} N_e/(N+1) \tag{12}$$

From eq 8, we get

$$\epsilon = b_A^2/b_e^2 \propto N_e/(N+1)b_e^2 \tag{13}$$

Thus the reduced spring constant ratio, defined as

$$\epsilon' \equiv \epsilon[(N+1)/N_e] \equiv \epsilon/\phi_A \propto 1/b_e^2 \tag{14}$$

is proportional to the inverse of the average dimensions of the effective submolecule connecting the slow beads through the medium.

Finally, we shall define a reduced relaxation time by first noting that the relaxation time in the RBZ model is

$$\tau_i = 1/2\sigma_B\lambda_i \tag{15}$$

where λ_i is the ith eigenvalue, and

$$\sigma_B = 3kT/b_B^2 f_B \tag{16}$$

In addition,

$$f_B = m\zeta = M\zeta/(N+1) \propto N_e/(N+1) \tag{17}$$

Combining eq 12 and 15–17 we find that $\tau_i = K\phi_A^2/\lambda_i$, where K is a lumped parameter, and from this define the reduced relaxation time

$$\tau_i' \equiv \tau_i/K = \phi_A^2/\lambda_i \tag{18}$$

The scale of these reduced relaxation times is substantially independent of our arbitrary choice of N, and their distribution is also independent of these choices as long as N is greater than approximately 20. Obviously, of course, the number of such relaxation times in the spectrum is equal to

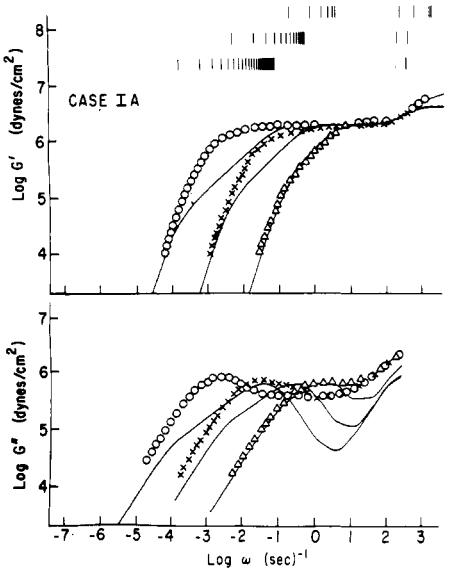

Figure 4. Double logarithmic plots of dynamic storage moduli G' and loss moduli G'' against measurement frequency in rad/s for a chain containing slow beads with uniformly enhanced friction coefficients and *no elastic coupling* (case IA). In this and subsequent figures through Figure 12, solid lines are computed curves, and triangles, crosses, and circles are the data of Onogi[20] for monodisperse polystyrene of molecular weights 1.13, 2.67, and 5.80 × 10^5, respectively. The discrete lines atop the figure represent the τ_i spectra predicted by the model for the cases considered, and their numerical values are given by the reciprocals of ω read from the abscissa.

N. In Table II, only the reduced values δ_A', ϵ', and $\Sigma\tau_i'$ are displayed for the cases studied here.

Results of the computations will be compared in most cases to the data of Onogi, Masuda, and Kitagawa[20] for monodisperse polystyrene, samples L37, L22, and L18 with M = 1.13, 2.67, and 5.8 × 10^5, respectively. We arbitrarily assume that entanglements are equally spaced along the chain (but not at the end positions) with a spacing determined by reported experimental values $M_e = M_c/2$. Porter and Johnson[1] cite a range 15 000 < M_e < 18 000 for polystyrene. Choosing $M_e \equiv$ 17 000 we ascertain that the three Onogi samples must contain N_e = 7, 16, and 34 entanglements, respectively. For illustration, the model is evaluated in some instances also for N_e = 4 and 2 (minimum possible for network formation) entanglements.

The total number of Gaussian statistical segments in the chain is somewhat arbitrary, equalling $N = (M/M_s)$ where the segment molecular weight M_s exceeds the Gaussian minimum; the number of beads in the molecule is $N+1$. Figures 1 and 2 show a repeating pattern of three beads in each entanglement sequence ($\nu = 3$), yielding M_s = 17 000/3 and $N + 1 = 3N_e + 2$. For this pattern, the three Onogi samples are represented by $N + 1$ = 23, 50, and 104. Table II shows that $\nu = 3$ was chosen for cases IIA1, IIC1, and IIC2, but even these moderate sizes of N can be reduced without influencing results. The rest of the cases in Table II utilized $\nu = 2$ for the two largest Onogi samples, so that $N + 1 = 2N_e + 1$ and matrix sizes are 33 and 69 rather than 50 and 104. This results in savings in computer time, and several trials showed that the predicted results are identical with those for $\nu = 3$. In our earlier work, it was found that the largest τ_i (of primary interest here) are insensitive to N for $N > 20$; changes in N are compensated in the mathematics by proportional changes in δ_A because f_B has changed, and in ϵ because b_B^2 has changed.

The data of Onogi are limited to the dynamical mechani-

Table II
Model Parameters for Entangled Polymers

Model	$N+1$	N_e	ϵ'	δ_A'	J_{eR}	$\Sigma\tau_i'$
			I. Enhanced Friction			
A. Uniform distribution	23	7	0	$0.70\ N_e^{2.28}$	0.436	3.40×10^2
–•–•–•–	33	16	0	$0.70\ N_e^{2.28}$	0.407	1.35×10^4
	69	34	0	$0.70\ N_e^{2.28}$	0.402	4.19×10^5
B. High-friction outside	23	7	0	$4.84\ (I)^{2.4}$	0.640	4.66×10^2
–●–•–•–•–●–	33	16	0	$4.84\ (I)^{2.4}$	0.640	1.27×10^4
	69	34	0	$4.84\ (I)^{2.4}$	0.640	3.47×10^5
C. High-friction inside	23	7	0	$14.3\ (I)^{2.4}$	0.364	4.07×10^2
–•–●–●–•–•	33	16	0	$14.3\ (I)^{2.4}$	0.322	1.43×10^4
	69	34	0	$14.3\ (I)^{2.4}$	0.310	3.75×10^5
			II. Elastically Coupled[a]			
A. Uniform distribution						
1. Moderate coupling	14	4	0.0165	$0.0654\ N_e^{3.75}$	0.479	1.33×10
	23	7	0.0165	$0.0654\ N_e^{3.75}$	0.356	4.02×10^2
	50	16	0.0165	$0.0654\ N_e^{3.75}$	0.138	1.84×10^4
	104	34	0.0165	$0.0654\ N_e^{3.75}$	0.046	9.30×10^5
2. Weak coupling	14	4	0.00328	$0.0750\ N_e^{3.45}$	0.488	1.19×10
	23	7	0.00328	$0.0750\ N_e^{3.45}$	0.415	3.15×10^2
	33	16	0.00328	$0.0750\ N_e^{3.45}$	0.251	1.50×10^4
	69	34	0.00328	$0.0750\ N_e^{3.45}$	0.092	6.92×10^5
B. High-friction outside						
1. Strong coupling	23	7	0.328	$0.758\ (I)^{5.2}$	0.514	3.58×10^2
	33	16	0.328	$0.758\ (I)^{5.2}$	0.213	1.46×10^4
	69	34	0.328	$0.758\ (I)^{5.2}$	0.103	8.34×10^5
2. Moderate coupling	23	7	0.0328	$0.205\ (I)^5$	0.690	2.90×10^2
	33	16	0.0328	$0.205\ (I)^5$	0.342	1.24×10^4
	69	34	0.0328	$0.205\ (I)^5$	0.131	7.21×10^5
C. High-friction inside						
1. Moderate coupling	14	4	0.0328	$4.81\ (I)^4$	0.630	2.30×10
	23	7	0.0328	$4.81\ (I)^4$	0.353	4.47×10^2
	50	16	0.0328	$4.81\ (I)^4$	0.188	2.90×10^4
	104	34	0.0328	$4.81\ (I)^4$	0.094	1.50×10^6
2. Weak coupling	14	4	0.00328	$5.80\ (I)^{3.4}$	0.568	2.20×10
	23	7	0.00328	$5.80\ (I)^{3.4}$	0.368	3.85×10^2
	50	16	0.00328	$5.80\ (I)^{3.4}$	0.237	2.22×10^4
	104	34	0.00328	$5.80\ (I)^{3.4}$	0.138	7.02×10^5

[a] Valves of ϵ' for Cases A, B, and C are chosen to give comparable fits to J_{er} data in Figure 16.

cal moduli. For stress relaxation data, we shall use those obtained by Akovali.[21,22] Specifically we used the data for the following three molecular weights, 1.25, 2.67, and 6.88 $\times 10^5$, which correspond to $N_e = 7$, 16, and 40, respectively.

Although Onogi's data appear to be the most comprehensive available in covering an extensive frequency region for a large number of molecular weights, it has been pointed out by Gupta, Shah, and Forsman[23] that the value of zero-shear viscosity obtained from the terminal zone of $G''(\omega)$ of the Onogi data appear to be inconsistent with those reported by over 13 groups of other investigators at corresponding temperatures. In addition, we note that their $G'(\omega)$ data are too flat in the rubbery plateau region; the stress relaxation data of Akovali[21] show a gradual but continuous decrease in $E_r(t)$ with increasing time, which is the expected behavior of uncrosslinked systems. These potential discrepancies in experimental data must be borne in mind when comparing them with the theoretical predictions.

Results

1. Dynamic Mechanical Properties. The dynamic mechanical moduli can be readily computed once the relaxation spectra are known (see Table I). In comparing with the experimental data, the theoretical curves are shifted vertically and horizontally until the rubbery plateau and rubber–glass transition regions coincide with the experimental curves.

In the enhanced friction model, δ_A is the only adjustable parameter. It can be seen in Figures 4–6 that the use of $\delta_A \gg 1$ has the effect of broadening the rubbery plateau region in $G'(\omega)$ and $G''(\omega)$ as desired. The case of uniform entanglement friction (δ_A = constant), which is case IA in Table II and is schematically represented as –•–•–•– (Figure 1b), was fitted to $G'(\omega)$ data as shown in Figure 4. The three theoretical curves were obtained by adjusting δ_A in each case until the far terminal region was fitted exactly. This procedure was equivalent to choosing a specific M dependence for δ_A which defines the breadth of the rubbery plateau. For Figure 4 it turns out that $\delta_A \sim M^{2.3}$, as could be expected in view of the well-established Ferry, Landel, and Williams procedure[8] of enhancing friction coefficients by a factor $Q \sim M^{2.4}$ in order to achieve broadening of the rubbery region.

Although the model is very successful for moderate-to-low M, as revealed by the almost perfect fit for L37, serious defects are revealed at higher M. The long flat shoulder with slope ½ (which reflects simply a Rouse τ_i spectrum in the long-time region, as represented discretely across the top of Figure 4) falls far under the real shoulder. This means also that the predictions of $\eta_0(M)$ and J_{eR} fail in exactly the same way as the conventional Rouse model. Another defect is apparent in Figure 4; the minima in the G'' plateau are much too deep, a deficiency shared to a lesser extent also by the Graessley[18] and Chömpff[9,10] theories.

Phenomenologically, the defects in Figure 4 would be remedied if the τ_i spectrum in the terminal zone were narrowed (building up the shoulder) and more τ_i were added to the early plateau region (raising the G'' minima). The latter is achieved if we introduce the very plausible physical case of position-dependent δ_A. These are just cases IB (–●–•–•–•–●–) and IC (–•–•–●–●–•–•–) of Table II, which

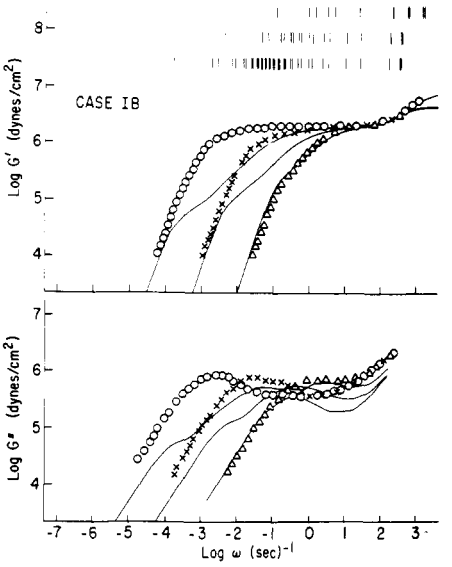

Figure 5. Double logarithmic plots of dynamic storage moduli G' and loss moduli G'' against measurement frequency for a chain containing slow beads with decreasing friction coefficients toward the chain interior and *no elastic coupling* (case IB).

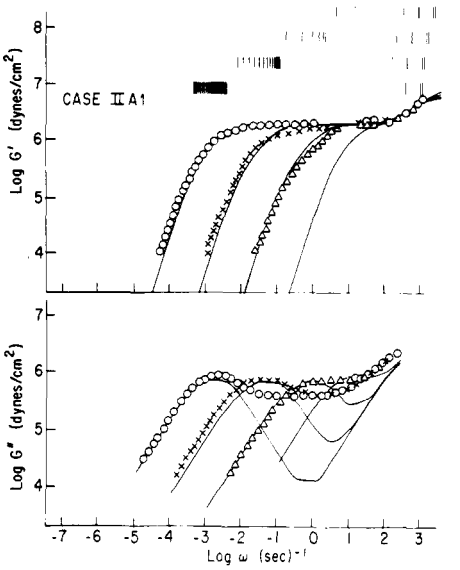

Figure 7. Double logarithmic plots of dynamic storage moduli G' and loss moduli G'' against measurement frequency for a chain containing slow beads with uniformly enhanced friction coefficients and *moderate elastic coupling* (case IIA1).

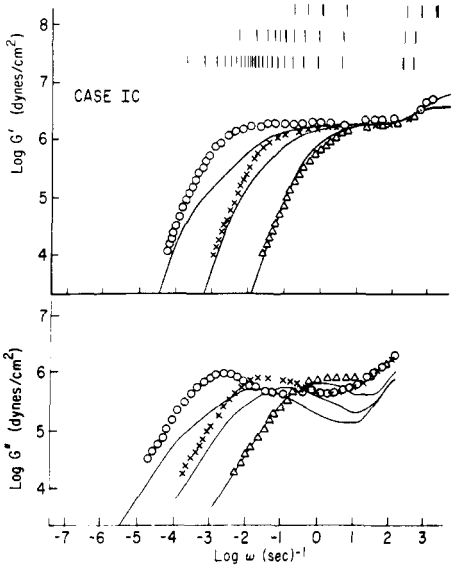

Figure 6. Double logarithmic plots of dynamic storage moduli G' and loss moduli G'' against measurement frequency for a chain containing slow beads with increasing friction coefficients toward the chain interior and *no elastic coupling* (case IC).

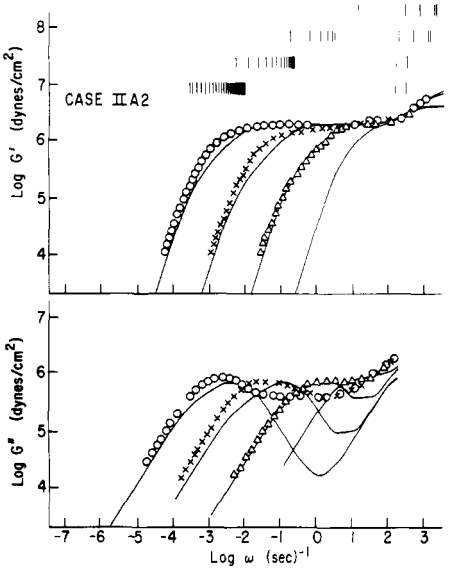

Figure 8. Double logarithmic plots of dynamic storage moduli G' and loss moduli G'' against measurement frequency for a chain containing slow beads with uniformly enhanced friction coefficients and *weak elastic coupling* (case IIA2).

correspond to the schematic diagrams of Figures 1c and 1d.

Results for these two cases are surprisingly similar and both represent some improvement, as seen in Figures 5 and 6, except in the far terminal zone. Case IB predicts a totally nonphysical extra shoulder at low ω on both G' and G'' curves, which was not shown in the graphical presentation of Chömpff and Prins.[10] This mismatch is particularly clear with sample L18. Earlier studies on block copolymers have shown that the presence of high-friction beads at the ends of the chains produces rather severe alterations in the terminal regions of the relaxation spectra by shifting the longest relaxation times farther away from the others.[16] This effect is clearly visible in the discrete τ_i spectra of Figure 5.

It is clear from Figures 4–6 that in the enhanced friction model, many of the same defects in fitting the terminal shoulder and in predicting η_0 and J_{eR} (to be described later), shared by previous models, are retained. Thus, we conclude that manipulating δ_A alone is inadequate to give a totally realistic representation of entanglement dynamics.

The addition of elastic coupling creates major qualitative improvements in all model predictions (Figures 7–12). Even with very weak coupling, marked benefits arise in fitting the $G'(\omega)$ shoulder for the uniform entanglement friction case (case IIA). The τ_i spectrum for sample L18 atop Figures 7 and 8 shows how a greater number of relaxation times in the terminal region causes the improved curve fit in the shoulder.

The effect of changing ϵ' for the uniform δ_A model is examined by taking $\epsilon' = 0.0165$ (case IIA1) and 0.00328 (case IIA2). From the G' and G'' curves in Figures 7 and 8, there seems to be no clear superiority between either. The larger ϵ' gives a better fit in the G' shoulder at high M, but the smaller ϵ' is somewhat superior at low M. Their G'' predic-

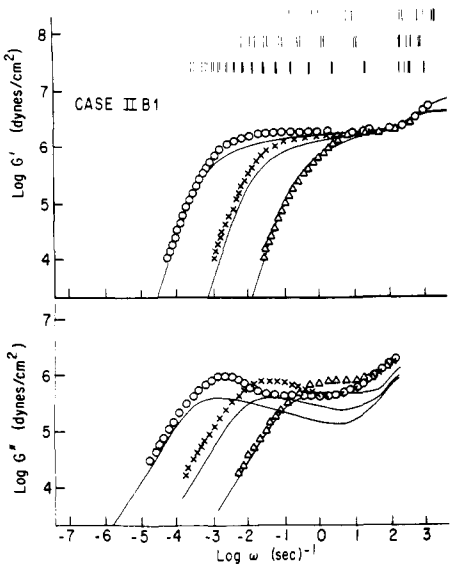

Figure 9. Double logarithmic plots of dynamic storage moduli G' and loss moduli G'' against measurement frequency for a chain containing slow beads with decreasing friction coefficients toward the chain interior and *strong elastic coupling* (case IIB1).

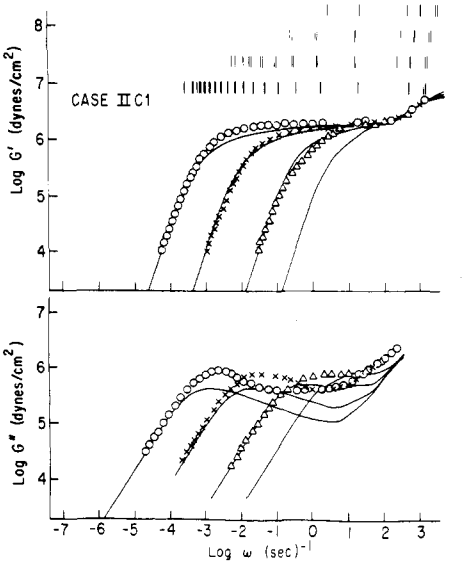

Figure 11. Double logarithmic plots of dynamic storage moduli G' and loss moduli G'' against measurement frequency for chains containing slow beads with increasing friction coefficients toward the chain interior and *moderate elastic coupling* (case IIC1).

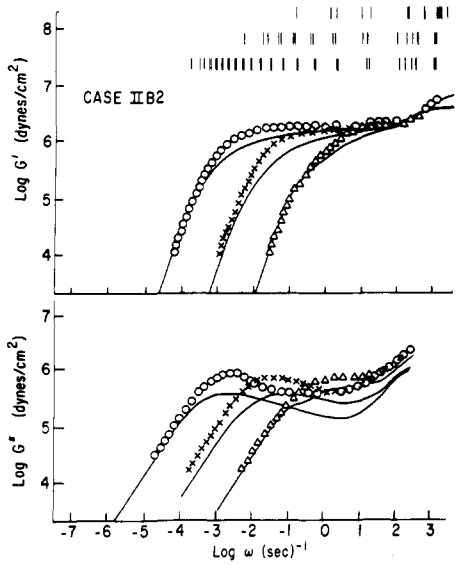

Figure 10. Double logarithmic plots of dynamic storage moduli G' and loss moduli G'' against measurement frequency for chains containing slow beads with decreasing friction coefficients toward the chain interior and *moderate elastic coupling* (case IIB2).

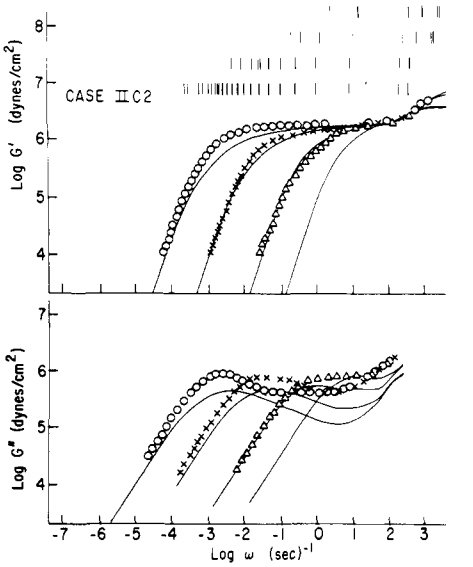

Figure 12. Double logarithmic plots of dynamic storage moduli G' and loss moduli G'' against measurement frequency for chains containing slow beads with increasing friction coefficients toward the chain interior and *weak elastic coupling* (case IIC2).

tions differ slightly in the flatness of their minimum troughs but have similar depths which are excessive, presumably due to using a constant δ_A rather than $\delta_A(I)$. However, the agreement between theory and experiment is excellent in the values of maximum G''. Overall, cases IIA must be classed as good fits and vastly superior to all cases without elastic coupling (cases I).

Values of δ_A were chosen separately to optimize the overall curve fit for each sample. This produced a relationship $\delta_A \sim M^{3.45}$ for case IIA2 and $M^{3.75}$ for case IIA1 which we used to generate the fourth curves in Figures 7 and 8 corresponding to $N_e = 4$ and $M = 68\,000$. No data for this molecular weight are available, but Onogi's other samples bracket it nicely.

Now turning our attention to the elastic coupling model with distributed entanglement friction coefficients, the computed $G'(\omega)$ and $G''(\omega)$ curves are compared with Onogi's data in Figures 9–12. The comparison was made by choosing a reasonable ϵ and then finding $\delta_A(I)$ described by eq 5, which offered the best fit for the three different molecular weights. The predicted $G'(\omega)$ curves are good for both slow-bead-outside (Figures 9 and 10) and slow-bead-inside models (Figures 11 and 12). The unrealistic shoulder at low frequencies shown in Figure 5 for the former vanishes when the coupling effect is introduced. The predicted $G''(\omega)$ minima are less severe than before, as desired, but the maxima also are less pronounced and lie lower than the experimental data. Both models are relatively insensitive to the magnitude of ϵ.

Considering the class II models, the evidence here seems to indicate that the elastic coupling can be very weak, with ϵ' being of the order of 10^{-3}, and the theory still produces quite good G' results. However, ϵ cannot be zero. As indicated in Figures 4–6, significant nonphysical predictions

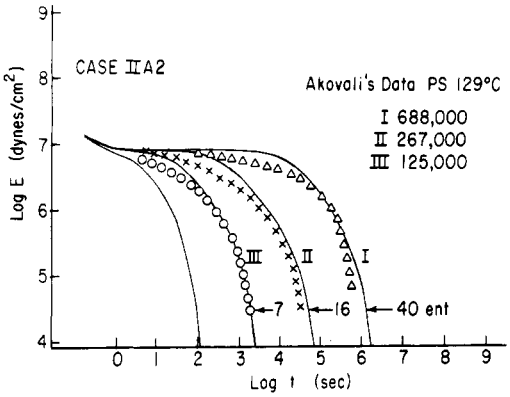

Figure 13. Double logarithmic plot of relaxation moduli, $E_r(t)$, against time for a chain containing slow beads with *uniformly enhanced* friction coefficients and weak elastic coupling (case IIA2). Solid lines are computed curves. Triangles, crosses, and circles represent the data of Akovali[21] for the monodisperse polystyrene of indicated molecular weights. The solid line for which no data were available for comparison was computed for four entanglements, which is equivalent to a molecular weight of 68 000.

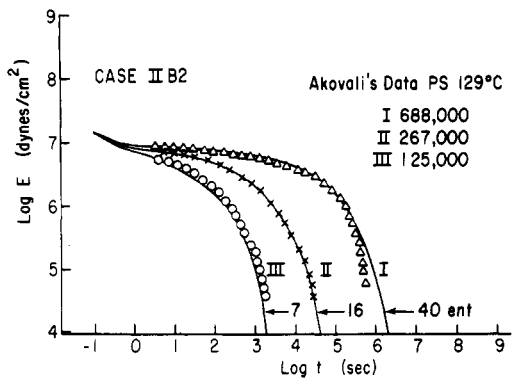

Figure 14. Double logarithmic plot of relaxation moduli, $E_r(t)$, against time for a chain containing slow beads with *decreasing friction coefficients* toward the interior of the chain and moderate elastic coupling (case IIB2).

are obtained when there is no intramolecular elastic coupling through the medium.

Although two parameters, δ_A and ϵ, are contained in the elastic coupling models, our experience with data suggests that they may not be independently adjustable. Using $\delta_A = aI^b$, we note that the subjective best data fits for each class (see IIB and IIC in Table II) yield values of b which are related to ϵ. As larger values of ϵ are chosen, b must also increase in order to achieve optimal curve fits. The correlation $b = 4.75 + \log \epsilon^{1/2}$, for instance, was obtained for case IIC from four choices of ϵ (only two given here). The corresponding values of a exhibited less regularity in their variation but, especially for IIC, did not vary strongly. This suggests a curve-fitting strategy wherein a would be fixed for the model (IIB or IIC) and only ϵ allowed to vary. For monodisperse polystyrene, then, only *one* independent adjustable parameter would exist here, as in the relatively naive enhanced friction model (case I).

2. Other Mechanical Properties. The theory can also predict other viscoelastic parameters, once the relaxation spectrum can be calculated (Table I). The tensile stress relaxation modulus $E_r(t)$ was computed and compared with the Akovali data. This procedure reconfirmed that an elastic coupling coefficient ϵ' is needed to give reasonable fits to data. Furthermore, the *distributed* δ_A (I) models (cases IIB and IIC) were again superior to the constant δ_A model (case

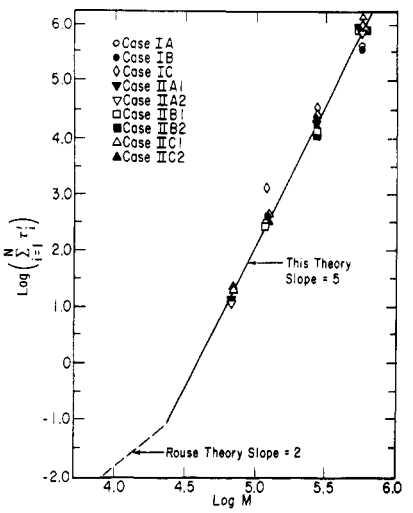

Figure 15. Double logarithmic plot of the summation of relaxation times ($\propto \eta_0 M$) against molecular weight. Points were computed, with the solid line drawn through them. The Rouse prediction for unentangled polymers is included as a broken line for comparison.

IIA), as demonstrated by the contrast of Figures 13 and 14; a major improvement is noted in the rubbery plateau. In general, $E_r(t) = 3G_r(t)$ comparisons for each model had success comparable to the $G'(\omega)$ comparisons, as expected, since $G_r(t)$ is essentially identical with $G'(\omega)$ when plotted on $1/t \approx \omega$ axis. These computed curves are shown simply for the sake of comparison with another set of literature data.[21]

Another viscoelastic parameter to be examined is the zero-shear-rate viscosity, η_0. By virtue of selecting δ_A and ϵ so that the terminal regions of $G'(\omega)$ are matched, we are assured of reasonable η_0 predictions. All variations of the model discussed here are shown in Figure 15. Most of the computed points fall on the straight line of slope 5.0. Some deviations, however, are noted for the uncoupled models (cases I). Since $\Sigma\tau_i \propto \eta_0 M$, the theory actually predicts $\eta_0 \sim M^{4.0}$ when $M > M_c$. Also included as a dashed line is the Rouse prediction of zero-shear viscosity for $M < M_c$, with a slope corresponding to $\eta_0 \sim M$.

The most interesting computed viscoelastic parameter to be compared with experimental data is the steady state shear compliance, J_e. Graessley[3] has collected such data for monodisperse polystyrene as computed from many types of measurements, and we present in Figures 16a–d the envelope of his plot (his Figure 5.15) of the reduced parameter $J_{eR} = J_e(\rho RT/M)$ vs. M. Superimposed on Figure 16a are the J_{eR} predictions of three noncoupled cases (cases I), which obviously fail. Far superior, as seen in Figure 16b, are the coupled systems with uniform entanglement friction (cases IIA). The latter, remarkably, predict a *maximum* which is strongly suggested by the accumulated data. Apparently no other mechanistic model has achieved this, although Janeschitz-Kriegl[24] pointed out that a separated set of relaxations at long times would lead to such a maximum. A defect in the case IIA predictions is that high M predictions cannot achieve simultaneously proper slope and magnitude; choices of ϵ' in Figure 16b satisfied magnitude but not slope. Data for several polymers[3] including polystyrene (and with a range now extended[25] to $M = 4.4 \times 10^7$) show that $J_{eR} \sim M^{-1}$ at high M, and the model predictions drop off faster than this in Figure 16b.

However, Figures 16c and 16d for the coupled systems with *distributed* entanglement friction coefficients show more realistic behavior; correct predictions are made of J_{eR} magnitude and slope at high M. The slow-bead-inside

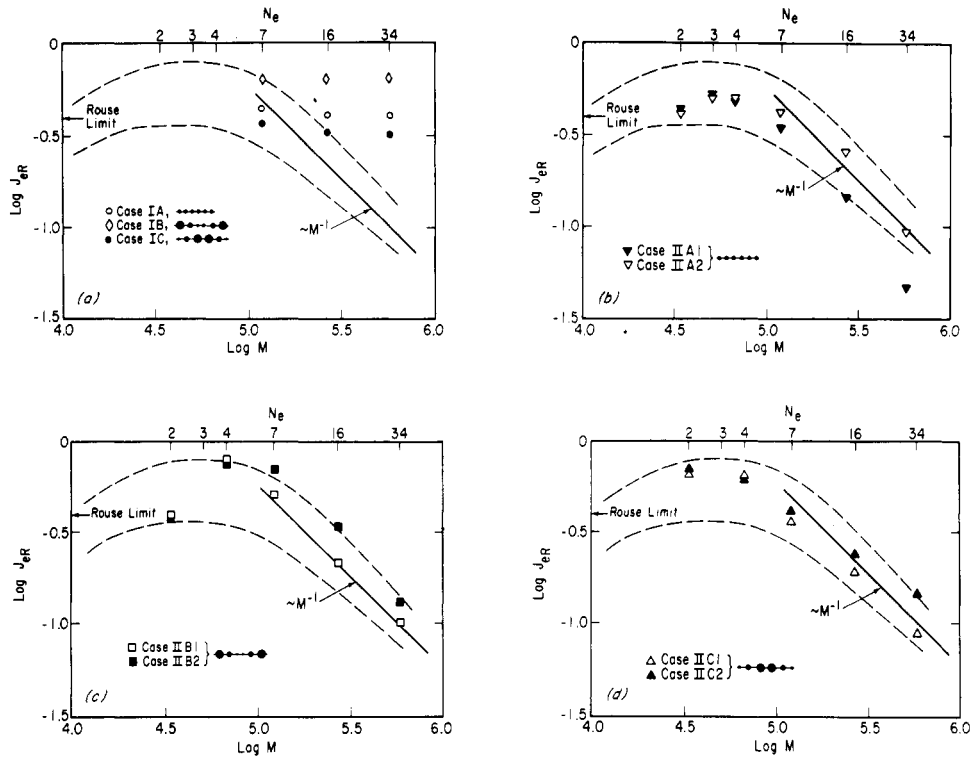

Figure 16. Double logarithmic plot of the reduced steady state shear compliance against molecular weight. Points were computed for cases indicated in the figure. The broken line brackets the literature data for monodisperse polystyrene collected by Graessley,[3] and the solid line provides a reference slope of −1 for testing whether $J_{eR} \sim M^{-1}$ at high M: (a) cases I; (b) cases IIA; (c) cases IIB; (d) cases IIC.

model (case IIC, Figure 16d) seems to be even better than the slow-bead-outside model (case IIB, Figure 16c), as the latter shows a rather precipitous drop in J_{eR} as $M \rightarrow M_c$. Case IIC1 seems to be better than IIC2 as the latter appears headed out of the envelope at high M, but both exhibit the maximum in a reasonable way and are consistent with the Rouse limit of $J_{eR} = 0.4$ for unentangled polymers.

The plot of J_{eR} vs. M is particularly useful in determining the limits of the range of ϵ'. Figures 16b–d show collectively that increasing ϵ' serves to reduce high M values of J_{eR}, also making the slope steeper. For each model, only a small range of ϵ' can be used to predict J_{eR} within the Graessley data band and also the $J_{eR} \sim M^{-1}$ approximation.

Discussion

The present model enjoys great success in predicting realistically all available linear viscoelastic properties, with only two independent parameters needed to characterize entanglement properties: the relative friction coefficient $\delta_A = f_A/f_B$ which determines the breadth of the rubbery plateau, and the relative elastic coupling coefficient ϵ which permits realistic fitting of the rubbery $G'(\omega)$ shoulder, $J_e(M)$ and $\eta_0(M)$. There is some evidence that the generalization $\delta_A = aI^b$ (–•–●–●–•–) is optimal, and moreover that a may be constant and $b = b(\epsilon)$ so that only *one* independent curve-fitting parameter is needed (at least, for the data examined here for monodisperse polystyrene).

The scheme described here for equal elastic coupling between all entanglements along the parent molecule is certainly not the only reasonable one. Other topological arrangements, such as position-dependent $\epsilon(I)$, can be envisioned. One version of this would be direct pairwise interaction along the chain, representing intramolecular entanglements which would be stronger than the present case wherein the interaction is propagated more weakly through the entanglement medium. Exploration of such pairwise "internal" entanglements is now in progress. Another version of position-dependent $\epsilon(I)$ would have a systematic variation with entanglement separation distance; this would be analogous to Zimm's dilute-solution analysis of position-dependent hydrodynamic interaction between all units of the chain.[6] Still another topology would be the totally uncoordinated springs of Graessley.[18]

An underlying presumption of the model is that complex polymer network dynamics can be phenomenologically interpreted in terms of their effect on individual chain dynamics. Although no rigorous justification can be presented for this at the present time, it is a helpful concept which permits employment of well-accepted mathematical and physical formalisms. With addition of the new elastic coupling proposed here, these formalisms lead to physical property predictions which are entirely compatible with data. It should also be pointed out that any model which assumes that entanglements operate at fixed points along the chain is physically inaccurate, since the entanglements are always sliding and changing position. Some defects in this concept have been emphasized by Ziabicki,[26] among them the impossibility of achieving normal-coordinate solutions to the dynamical problem and meaningful eigenvalues. Despite these fundamental objections, we present our present model in the spirit of a time average of entanglement positions and dynamics and contend that its success reflects the utility of such modeling.

In conclusion, we have in this paper demonstrated the importance of taking into account the effect of intramolecular elastic coupling along the parent chain through the medium of passing chains. Modeling the entanglement effects solely by enhanced frictional coefficients at the entanglement points is inadequate in predicting the various properties. By comparison with the experimental data of $G'(\omega)$, $G''(\omega)$, $E_r(t)$, η_0, and particularly J_{eR}, we find that in

all the cases studied here, the best model is case IIC1 which has distributed slow beads with the slowest beads in the interior of the chain and elastically coupled via the medium with a spring constant approximately 10^{-2} that for the in-chain entropy springs.

Acknowledgment. This work was supported by the Office of Naval Research.

References and Notes

(1) R. S. Porter and J. F. Johnson, *Chem. Rev.*, **66**, 1511 (1966).
(2) J. D. Ferry, "Viscoelastic Properties of Polymers", 2nd ed, Wiley, New York, N.Y., 1970.
(3) W. W. Graessley, *Adv. Polym. Sci.*, **16**, 1 (1974).
(4) P. E. Rouse, *J. Chem. Phys.*, **21**, 1272 (1953).
(5) F. Bueche, *J. Chem. Phys.*, **22**, 603 (1954).
(6) B. Zimm, *J. Chem. Phys.*, **24**, 269 (1956).
(7) F. Bueche, *J. Chem. Phys.*, **20**, 1959 (1952); *ibid.*, **25**, 599 (1956); *ibid.*, **40**, 484 (1964).
(8) J. D. Ferry, R. F. Landel, and M. L. Williams, *J. Appl. Phys.*, **26**, 359 (1955).
(9) A. J. Chömpff and J. A. Duiser, *J. Chem. Phys.*, **45**, 1505 (1966).
(10) A. J. Chömpff and W. Prins, *J. Chem. Phys.*, **48**, 235 (1968).
(11) P. G. DeGennes, *J. Chem. Phys.*, **55**, 572 (1971).
(12) G. V. Vinogradov, V. H. Pokrovsky, and Yu. G. Yanovsky, *Rheol. Acta*, **11**, 258 (1972).
(13) R. S. Marvin and H. Oser, *J. Res. Natl. Bur. Stand., Sect. B*, **66**, 171 (1962); *ibid.*, **67**, 87 (1963).
(14) R. E. DeWames, W. F. Hall, Jr., and M. Shen, *J. Chem. Phys.*, **46**, 2782 (1967).
(15) M. Shen and D. R. Hansen, *J. Polym. Sci., Polym. Symp.*, **46**, 55 (1974).
(16) D. R. Hansen and M. Shen, *Macromolecules*, **8**, 343 (1975); *ibid.*, **8**, 903 (1975).
(17) J. J. Aklonis, W. J. MacKnight, and M. Shen, "Introduction to Polymer Viscoelasticity", Wiley, New York, N.Y., 1972.
(18) W. W. Graessley, *J. Chem. Phys.*, **47**, 1942 (1967); *ibid.*, **54**, 5143 (1971).
(19) W. C. Forsman and H. S. Grand, *Macromolecules*, **5**, 289 (1972).
(20) S. Onogi, T. Masuda, and K. Kitagawa, *Macromolecules*, **3**, 109 (1970).
(21) G. Akovali, *J. Polym. Sci., Part A-2*, **5**, 875 (1967).
(22) A. V. Tobolsky, J. J. Aklonis, and G. Akovali, *J. Chem. Phys.*, **42**, 723 (1965).
(23) S. Gupta, V. R. Shah, and W. C. Forsman, *Macromolecules*, **7**, 948 (1974).
(24) H. Janeschitz-Kriegl, *Adv. Polym. Sci.*, **6**, 170 (1969).
(25) N. Raghupathi and D. J. Plazek, paper at the Society of Rheology Meeting, St. Louis, Oct. 1975.
(26) A. Ziabicki, *Macromolecules*, **7**, 501 (1974).

NMR Relaxation Time Studies of Polystyrene

Michael F. Froix,* D. J. Williams, and Andreas O. Goedde

Xerox Corporation, Webster, New York 14580. *Received October 20, 1975*

ABSTRACT: Proton spin–lattice (T_1) and spin–spin (T_2) relaxation times are reported for polystyrene (PS) samples of low (10 K) and high (2×10^6) molecular weights and varying surface areas in oxygen, ambient, and in vacuo. The measurements were made in order to elucidate the molecular dynamics responsible for the various NMR and dielectric relaxation processes in PS and so clarify several sources of discrepancy in earlier literature data and interpretation. Correlation frequencies are determined from NMR data as well as data from other sources in the literature. A molecular weight dependent α relaxation was observed which is in good agreement with previously reported data. Variations in the positions and intensities of low-temperature T_1 data are traced to spin diffusion to end groups and either direct relaxation by O_2 or spin diffusion to O_2 or a combination of these. The intrinsic γ relaxation is observed in the T_1 data but in the T_2 data only in the presence of O_2. By analogy with poly(*n*-vinylcarbazole) the γ process is attributed to low-amplitude torsional libration of the phenyl group. At low temperatures O_2 contributes to the dipolar field causing a reduction in T_2. Above the temperature corresponding to about 10^4 Hz for the γ relaxation, the lifetime of the O_2 phenyl ring complex is short and rapid relative reorientation of O_2 with respect to the proton spin system causes an increase in T_2. As a result there is a change in the T_1 mechanism from spin diffusion to direct paramagnetic relaxation by the diffusing O_2 molecules.

A large volume of molecular relaxation data obtained from dielectric, mechanical, and nuclear magnetic resonance (NMR) techniques has been accumulated on the molecular motions of polystyrene (PS). These techniques have revealed the existence of multiple relaxations. With the exception of the glass transition (α relaxation) there appears to be considerable disagreement on the interpretation of the relaxation time data.

Dynamic mechanical[1] and dielectric[1] relaxation of PS samples including thermally degraded samples have shown five relaxations below the glass transition at a frequency of 10 kHz. The β relaxation found at 360 K is attributed to local oscillation of backbone chains while the γ peak at 180 K due to phenyl rotation is observed only in the mechanical measurements. The γ' peak at 100 K is observed only in the dielectric relaxation of bulk polymerized samples and is assigned to the motion of weak polar bonds involving oxygen atoms in the chain. A peak at 55 K in dynamic mechanical measurements is believed to result from lattice defects caused by the placement of a syndiotactic diad between isotactic sequences or vice versa. The relaxation mechanism for the newly reported ϵ peak at 25 K is not known.

The NMR data on PS exhibit considerable variation in the number of transitions, the temperature at which they occur, and the assignment of the molecular processes responsible for them. The available data are voluminous and no attempt will be made here to review them; however, the conclusions of some of the more widely referenced studies will be discussed. Hunt, Powles, and Woodward[2] measured the spin–lattice relaxation times (T_1) of PS as a function of temperature. Three relaxations corresponding to T_1 minima at $\simeq$500, 260, and 130 K were observed. The high-temperature minimum was identified with the α process. By comparing polystyrene with poly(phenyl-L-alanine) it was suggested that the low-temperature minima might be due either to oscillation of the phenyl ring or to reorientational motion of impurities such as residual monomer which could lead to relaxation of the polymer by spin diffusion, or to a combination of these two processes. Examination of PS sample purified by reprecipitation from toluene with methanol and dried in vacuum showed T_1 behavior above 300 K similar to that of the previous sample. However, a deep minimum which was observed at 160 K disappeared on heating to 520 K and the repeated T_1 plot was now similar to that of the previous sample. The authors con-